N O T E

TURBINE-MRE: A 3D hybrid radial-Cartesian EPI acquisition for MR elastography

Yi Sui[1] (iD) | **Arvin Arani[1]** | **Joshua D. Trzasko[1]** | **Matthew C. Murphy[1]** |
Phillip J. Rossman[1] | **Kevin J. Glaser[1]** | **Kiaran P. McGee[1]** | **Armando Manduca[2]** (iD) |
Richard L. Ehman[1] | **Philip A. Araoz[1]** | **John Huston III[1]**

[1]Department of Radiology, Mayo Clinic, Rochester, Minnesota, USA

[2]Department of Physiology & Biomedical Engineering, Mayo Clinic, Rochester, Minnesota, USA

Correspondence
Yi Sui, Department of Radiology, Mayo Clinic, 200 First Street SW, MN 55905, USA.
Email: sui.yi@mayo.edu

Purpose: To develop a novel magnetic resonance elastography (MRE) acquisition using a hybrid radial EPI readout scheme (TURBINE), and to demonstrate its feasibility to obtain wave images and stiffness maps in a phantom and in vivo brain.

Method: The proposed 3D TURBINE-MRE is based on a spoiled gradient-echo MRE sequence with the EPI readout radially rotating about the phase-encoding axis to sample a full 3D k-space. A polyvinyl chloride phantom and 6 volunteers were scanned on a compact 3T GE scanner with a 32-channel head coil at 80 Hz and 60 Hz external vibration, respectively. For comparison, a standard 2D, multislice, spin-echo (SE) EPI-MRE acquisition was also performed with the same motion encoding and resolution. The TURBINE-MRE images were off-line reconstructed with iterative SENSE algorithm. The regional ROI analysis was performed on the 6 volunteers, and the median stiffness values were compared between SE-EPI-MRE and TURBINE-MRE.

Results: The 3D wave-field images and the generated stiffness maps were comparable between TURBINE-MRE and standard SE-EPI-MRE for the phantom and the volunteers. The Bland–Altman plot showed no significant difference in the median regional stiffness values between the two methods. The stiffness measured with the 2 methods had a strong linear relationship with a Pearson correlation coefficient of 0.943.

Conclusion: We demonstrated the feasibility of the new TURBINE-MRE sequence for acquiring the desired 3D wave-field data and stiffness maps in a phantom and in-vivo brains. This pilot study encourages further exploration of TURBINE-MRE for functional MRE, free-breathing abdominal MRE, and cardiac MRE applications.

K E Y W O R D S
MR elastography, radial acquisition, TURBINE

1 | INTRODUCTION

Magnetic resonance elastography (MRE) is a non-invasive imaging method to assess tissue stiffness by measuring the propagating shear waves induced by external harmonic vibration. The shear wave motion is encoded in the MR phase signals using motion encoding gradients before the readout. The 2D spin-echo EPI sequence has been widely used for MRE acquisitions in the brain, liver, and heart[1] to study the tissue stiffness in static states.[2] In more recent studies, there are increasing interests to investigate the dynamic changes of brain tissue viscoelasticity related to cerebral arterial pulsation,[3] or to detect fast neuronal activity using functional MR Elastography.[4,5] A high temporal resolution and physiological-motion resolved MRE is desired in these applications. However, the current 2D Cartesian acquisition typically used in MRE may face challenges for such applications because of its low temporal resolution and lack of self-navigation to resolve the physiological motion.

Recently, a 3D hybrid radial-EPI readout scheme (TURBINE) was proposed,[6–9] in which the EPI planes are rotated by different angles about the phase-encoding axis. The 3D k-space is radially sampled in the off-axis dimensions and Cartesian sampled in the EPI planes. The partial radial acquisition scheme in TURBINE provides the potential to achieve motion robustness and higher temporal resolution when combined with golden-angle scheme, sliding window view-sharing technique,[8] and advanced reconstruction algorithms.[10]

To date, the TURBINE technique has been successfully applied to DWI[6] and fMRI[7] that only display and process magnitude information. However, its ability to obtain phase images, which is essential for MRE, has not been demonstrated. In this preliminary work, we developed the new TURBINE-MRE sequence and demonstrated its feasibility in a phantom and an in vivo brain study as the first step toward the future advanced applications.

2 | METHODS

2.1 | Pulse sequence

The proposed TURBINE-MRE acquisition strategy is based on a spoiled gradient-echo MRE sequence with a modified EPI readout, as shown in Figure 1A. MRE motion-encoding gradients (MEGs) were added before the EPI readout to encode MRE harmonic tissue motion into the phase image. They can be applied on the x, y, and/or z axes to record the full harmonic displacement field. The triggering of the mechanical vibration was temporally shifted with respect to the MEGs by a time delay (φ) in each acquisition to acquire wave images at different phases of the harmonic motion. To achieve the TURBINE acquisition, the EPI readout axis, G_θ, rotated about the slab-selective (G_{SS})/phase-encoding (G_{PE}) axis in successive TRs. One 2D plane within the target 3D k-space was sampled with the EPI trajectory (TURBINE blade) during each TR (Figure 1B). To cover the entire 3D k-space, the sampling plane was angularly rotated by a fixed increment before each repetition. The angular sampling can be evenly distributed over 180° or distributed with a golden angle increment.

2.2 | Phantom experiment

A polyvinyl chloride (PVC) brain phantom with sphere inclusions[11] was scanned on a compact 3T scanner (GE Healthcare, Waukesha, WI; DV26 R02)[12–14] with a 32-channel head coil (Nova Medical, MA). An external vibration at 80 Hz was applied in the y-direction (AP direction), which was also selected as the slab-selective (G_{SS})/phase-encoding (G_{PE}) axis. The imaging parameters were: TR/TE = 50/18.5 ms, flip angle = 20°, slab thickness = 140 mm, EPI FOV = 240 (read) × 180 (phase) mm^2, acquisition matrix = 96 × 72
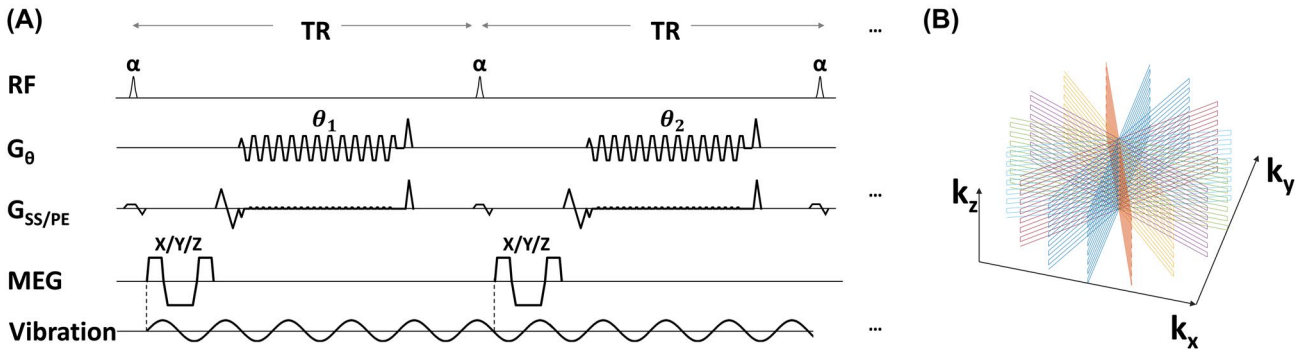

FIGURE 1 (A) Pulse sequence diagram for TURBINE-MRE. The MEG can be applied in the x, y, and/or z directions to record the full vector wave motion. The MEG and the mechanical vibration are temporally shifted relative to each other to acquire different phase offsets of the harmonic motion. $G_{SS/PE}$ represents the slab-selection axis and EPI phase-encoding direction. G_θ represents the readout axis rotating about the $G_{SS/PE}$ axis in successive TRs. (B) The 3D TURBINE k-space trajectory. An EPI readout (blade) is acquired in each TR. Successive EPI readouts are rotated along the $G_{SS/PE}$ axis (k_z in this case) to fill k-space

and phase-encoding acceleration factor of 3, and 192 radial-encoding positions were scanned with a golden angle (111.248°) increments. A 12.5-ms gradient-moment-nulled (GMN) MEG was applied at 80 mT/m amplitude yielding a motion encoding efficiency (Menc) of 10.0 μm/π-radians. The reconstructed image spatial resolution was an isotropic 2.5 mm. The total scan time per 3D volume was 9.6 s, or 3:50 min for a complete MRE data set with 6 motion-encoding directions ($\pm$X, $\pm$Y, and $\pm$Z) and 4 time offsets (24 of 3D volumes total). A standard 2D, multislice, spin-echo (SE) EPI-MRE acquisition was also performed as a reference approach with TR/TE = 3000/38.9 ms, acquisition matrix = 96 × 96, slice thickness = 2.5 mm, two balanced MEGs with Menc = 5.0 μm/π-radians, 6 motion-encoding directions, 8 phase offsets, and a total scan time of 3:12 min.

2.3 | In vivo experiments

With IRB approval and informed consent, 6 normal, healthy volunteers were scanned with the same setup as the phantom study except a 60 Hz vibration was used to compensate for the wave damping in the brain. The in vivo imaging parameters for the TURBINE-MRE were TR/TE = 50/22.7 ms, flip angle = 15°, Menc = 7.8 μm/π-radians, and scan time 3:50 min; whereas for the SE-EPI-MRE, TR/TE = 4667/62.4 ms, number of slices = 56, Menc = 3.9 μm/π-radians, and scan time of 3:49 min. The other imaging parameters were otherwise the same as those in the phantom experiments aforementioned.

2.4 | Image reconstruction and post-processing

Non-phase encoded reference k-space lines were acquired before actual scans for each EPI blades at the same radial angles. One-dimensional zero and first-order phase correction was applied before variable readout gradient filtering (VRGF) resampling on every EPI blade to minimize the Nyquist ghost[15,16] using Orchestra software development kit (version 1.7; GE Healthcare) for MATLAB. All EPI blades associated with a single temporal state were first combined on a per-channel basis to form a 3D k-space quantity for each, and then Tikhonov-regularized SENSE reconstruction[17,18] (ie, linear least squares estimation) was performed on each undersampled multi-coil 3D radial-Cartesian TURBINE data set via conjugate-gradient iteration. The number of iterations was fixed at 40. Discrete-space Fourier transform (DSFT) operations implicit within the SENSE acquisition model were executed using the non-uniform FFT (NUFFT) with 6 × 6 Kaiser-Bessel kernel and 1.5× oversampling ratio.[19] Coil sensitivity profiles were estimated from a separate calibration scan using a gradient-echo sequence. The Tikhonov regularization parameter was manually selected as $\lambda = 0.001$ for all experiments.

MRE stiffness maps were generated by adaptively taking the curl of the 3D displacement field, smoothing the curl images, and performing a 3D direct inversion (DI) algorithm to invert the wave-field as described in the previous study.[20,21]

To study the acceleration potential of TURBINE-MRE, a subset of the EPI blades (the first N blades) was used for image reconstruction and MRE inversion, where $N = 16$, 32, 64, 96, 128, or 160.

All the image reconstruction and MRE stiffness calculations were performed off-line in 64-bit MATLAB (The MathWorks, Natick, MA) on a Linux workstation with two 12-core Intel Xeon E5-2650 v4 CPUs running at 2.2 GHz and 64 GB system memory.

2.5 | Brain regional stiffness calculation

The regional brain stiffness analysis was done in a similar approach as described in the previous study.[21] Briefly, 6 regional ROIs—including the cerebrum, frontal lobes, occipital lobes, parietal lobes, temporal lobes, and the cerebellum—were generated from 3D MP-RAGE T_1-weighted images, and ROIs were then registered to MRE magnitude images and propagated to stiffness maps. The median stiffness values in each ROI were used for comparison. Bland–Altman analysis and Pearson correlation were used to assess agreement between SE-EPI-MRE and TURBINE-MRE.

2.6 | Results

Figure 2 compares the phantom results between SE-EPI-MRE and TURBINE-MRE. The magnitude images are shown in Figure 2A with axial, sagittal, and coronal views. The curl wave images (only x component of the curl vector is shown) in Figure 2B are visually comparable between the two methods. Of note, TURBINE-MRE was a true 3D acquisition, while SE-EPI-MRE acquired a stack of 2D axial images which were later reformatted to sagittal and coronal views for display. The stiffness maps are shown in Figure 2C with the ROIs (dashed circles) placed on the inclusions. The locations of the 6 inclusions were also marked with asterisks on the structural images (Figure 2D). The median stiffness measured from the inclusion and the backgrounds were 5.27 kPa and 3.88 kPa, respectively, for SE-EPI-MRE, and 5.64 kPa and 3.99 kPa for TURBINE-MRE.

Figure 3 compares in vivo brain results between SE-EPI-MRE and TURBINE-MRE from 1 representative volunteer. Figure 3A shows the magnitude images of the 2 sequences. The SE-EPI-MRE showed T_2-weighted contrast between
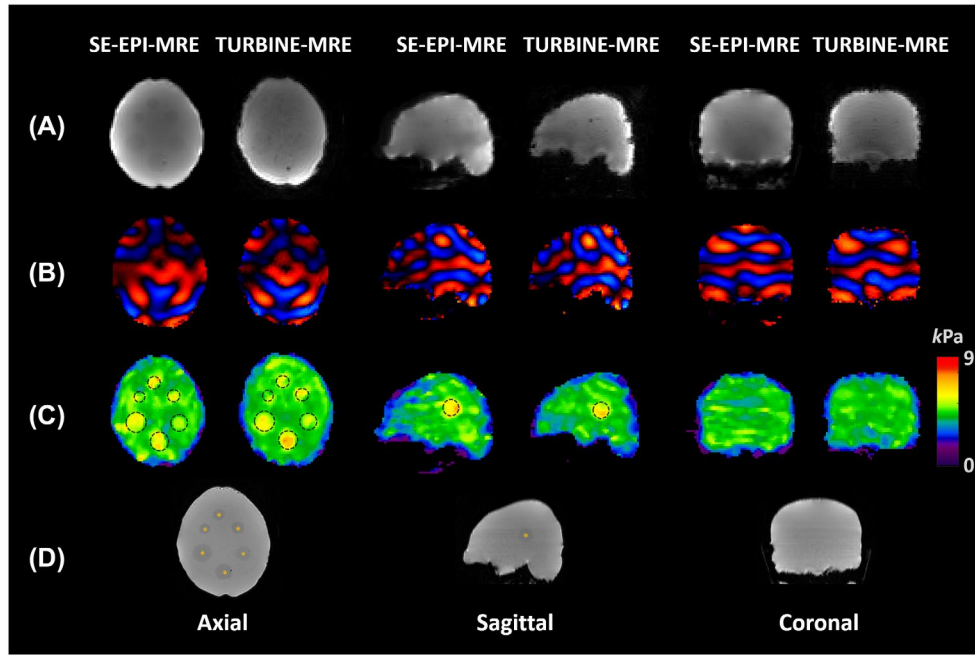
FIGURE 2 Phantom results from SE-EPI-MRE and TURBINE-MRE sequences in axial, sagittal, and coronal views. (A) Magnitude images. (B) x-component of the curl wave images. (C) Stiffness maps with 6 ROIs (dashed circles) placed on the inclusions. (D) Structural T_2-FSE images with the locations of the 6 inclusions indicated by asterisks
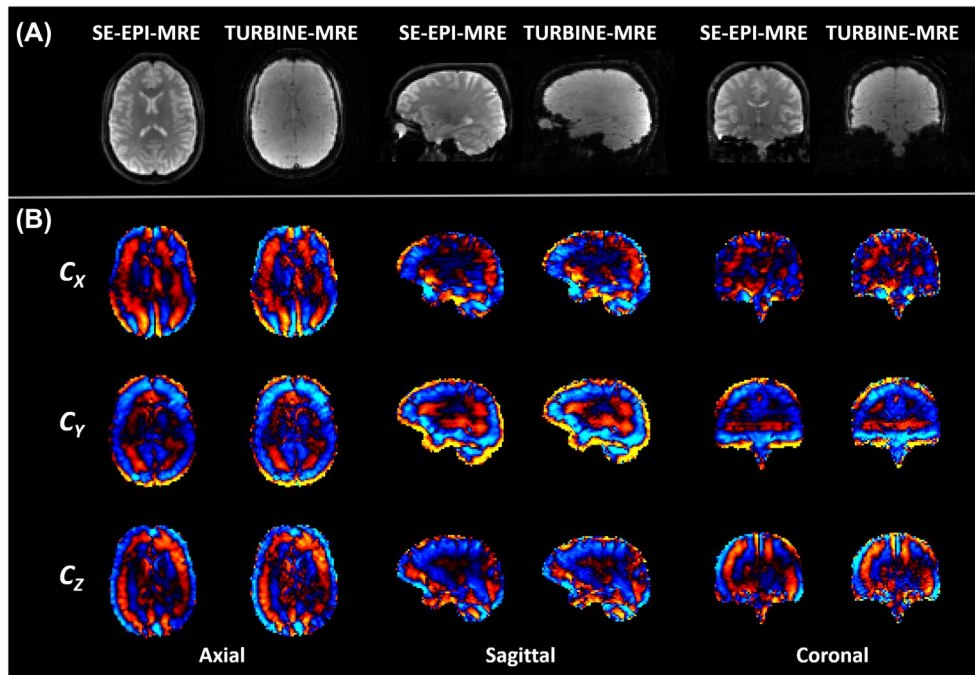

FIGURE 3 Representative volunteer results from the SE-EPI-MRE and TURBINE-MRE sequences in axial, sagittal, and coronal views. (A) Magnitude images. (B) x-, y-, and z-component (Cx, Cy, and Cz, respectively) of the curl wave images

gray and white matter, whereas TURBINE-MRE magnitude images have low contrast between tissues because the Ernst angle was chosen to maximize the signal intensity rather than the contrast. The wave images of SE-EPI-MRE and TURBINE-MRE are comparable as shown in Figure 3B. Of note, the standard slice de-jittering has been applied to the SE-EPI-MRE result to mitigate the slice-to-slice phase variation artifacts as described elsewhere.[21,22] In contrast, no de-jittering was needed for TURBINE-MRE, because it exhibited minimal slice-to-slice phase variation.

Figure 4 shows the MP-RAGE T_1-weighted anatomic images (Figure 4A) and the stiffness maps of SE-EPI-MRE
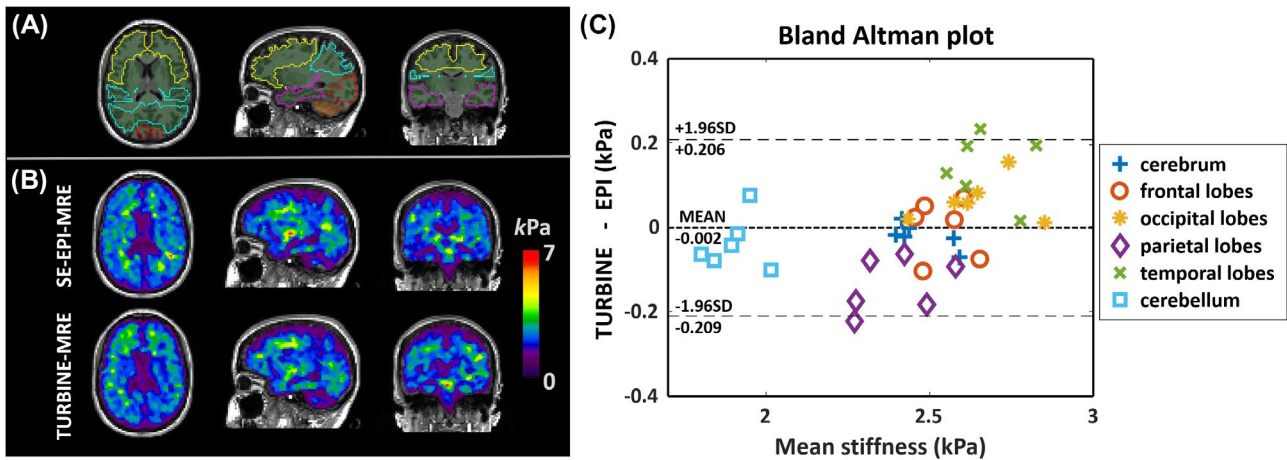
FIGURE 4 Regional stiffness analysis. (A) Six regional ROIs of the cerebrum (green patch), frontal lobes (yellow contour), occipital lobes (red), parietal lobes (cyan), temporal lobes (magenta), and the cerebellum (orange patch) were generated from MP-RAGE T_1-weighted images. (B) The ROIs were registered to MRE magnitude image and then propagated to stiffness maps obtained from SE-EPI-MRE and TURBINE-MRE. (C) The Bland-Altman plot of the median regional stiffness values from 6 volunteers
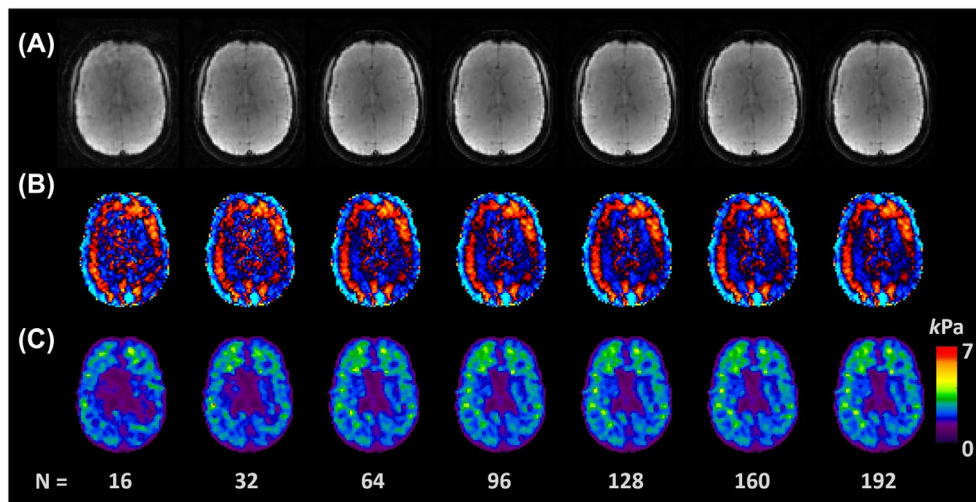

FIGURE 5 (A) The magnitude, (B) z-direction wave, and (C) stiffness images reconstructed using the different number N of EPI blades

and TURBINE-MRE (Figure 4B) from one representative volunteer. For each volunteer, 6 ROIs of the cerebrum (green patch), frontal lobes (yellow contour), occipital lobes (red contour), parietal lobes (cyan contour), temporal lobes (magenta contour), and the cerebellum (orange patch) were created from the T_1-weighted images. The ROIs were then registered to MRE magnitude images and then propagated to stiffness maps obtained from SE-EPI-MRE and TURBINE-MRE. Despite the low tissue contrast on TURBINE-MRE magnitude images, the registration algorithm[21] used in this study was able to accurately register T_1-weighted images to the magnitude images. All the registrations were visually confirmed by overlaying the registered T_1-weighted images and MRE magnitude images. The Bland–Altman plot (Figure 4C) showed no significant difference ($P < 0.05$) in the median regional stiffness values of the 6 volunteers between the 2 methods. The regional stiffness values measured from all

volunteers with the 2 methods had a strong linear relationship with a Pearson correlation coefficient of 0.943.

Figure 5 shows an example slice of the magnitude images (Figure 5A), z-component of the curl wave images (Figure 5B), and stiffness maps (Figure 5C) reconstructed using different numbers of blades. The median regional stiffness values obtained from N (16, 32, 64, 96, 128, or 160) blades were plotted against that of using all 192 blades on the scatter plots (see Supporting Information Figure S1). Under the acquisition and reconstruction setup described here, the stiffness values were evidently slightly underestimated when using a small number of blades (eg, $N = 16$ or 32). We hypothesize that this underestimation or downward bias is dominantly a result of our using a single regularization parameter value across all experimental setups, as this causes the effective degree of regularization to be (approximately) inversely proportional to sampling level.[23] However, at as few as 64 blades,

the stiffness estimation was already almost identical to that of 192 blades (r = 0.999), demonstrating the high acceleration capability of the TURBINE-MRE sequence.

3 | DISCUSSION

In this study, we developed a novel TURBINE-MRE method. The phase difference images were successfully reconstructed to obtain the wave displacement information. The phantom and in vivo brain results demonstrated the feasibility of TURBINE-MRE for acquiring 3D wave-field data. The whole brain volume data with a high spatial resolution (2.5 mm isotropic) can be collected within 4 min. The radially sampling scheme, together with the iterative reconstruction, demonstrated great potential to accelerate the acquisition meanwhile maintaining accurate stiffness estimation. In this study, only as few as 64 blades (a 1:20 min scan) was sufficient for a consistent stiffness measurement. We anticipate that migrating to an advanced nonlinear regularization model (eg, joint wavelet sparsity) within the reconstruction setup will enable comparable reconstruction accuracy to be obtained from even fewer blades, further reducing overall scan time.

The partially radial sampling strategy in TURBINE-MRE provides the sequence similar self-navigation property of radial imaging as described in the XD-GRASP method.[10] The EPI blades repeatedly sample the k-space center, allowing the extraction of respiratory and/or cardiac motion signals directly from the data. The blades can be retrospectively sorted into multiple discrete motion-states based on the motion signals. The golden-angle scheme causes the arbitrary data sorting to provide approximately uniform k-space coverage in each motion state. Usually, the k-space in each motion state is undersampled, so a compressed sensing type of reconstruction can be used to exploit sparsity both within the spatial dimensions and along the respiratory and/or cardiac motion dimension to mitigate the undersampling artifacts. Hence, with further development, the TURBINE-MRE sequence can be highly accelerated to be suitable for imaging fast dynamic stiffness changes and/or moving objects. This will particularly benefit the liver and cardiac MRE applications, which are usually performed with breath-hold sequences.[24] The breath-hold (typically 15–20 s) may impose difficulties for some patients; in addition, the inconsistent diaphragmatic position between breath-holds may result in misregistration errors for stiffness estimation.[25] The TURBINE-MRE sequence proposed and validated here provides a foundation on which a free-breathing, motion-resolved MRE acquisition could be built.

In our current implementation, a separate calibration scan was needed to estimate the coil sensitivity profiles. In the future, we will further explore the use of autocalibrating paradigms, which for TURBINE-MRE may include interleaving of additional EPI-based auto-calibration signal (ACS) passes within or between the primary TURBINE blades. From this auxiliary data, coil sensitivity profiles could be estimated either as part of the reconstruction process or using a pre-reconstruction procedure like ESPIRiT.[26] This would significantly reduce the risk of error propagation because of the mismatch between the separate calibration scan and the TURBINE scan because of motions, improving overall SNR and reducing residual artifacts.

The slice-by-slice phase variation artifact or slice jitter is commonly seen in 2D multi-slice MRE from various causes such as patient movement or physiological movement throughout the scan. This artifact manifests as spatially low-order phase terms, which, if not corrected before MRE processing, will alter the apparent wavelength along the slice direction, leading to a severe error in stiffness estimation. This artifact may be corrected by high-pass filtering the 2D slices of complex wave data, as done in this and previous studies,[21,22] or by alternative processing techniques.[27,28] In 3D TURBINE acquisition, the phase errors are present between EPI blades in k-space instead of 2D slices (image space) in a dispersed and incoherent manner; therefore, they are not as visually apparent and have less impact on the stiffness estimation. We did not attempt to correct the phase error at this stage because it did not visually appear to corrupt the TURBINE images. Still, we plan to quantify and, if needed, develop a correction process for these terms in the future.

In this study, SE-EPI-MRE was chosen as a reference approach to validate our 3D TURBINE-MRE by comparing the wave images and stiffness measurement. SE-EPI-MRE has been reliably used in many previous brain-MRE studies and is routinely used in our clinical practice because of its rapid acquisition schemes and high motion-sensitivity.[2,29] A more similar sequence such as 3D gradient-echo MRE could be used for comparison. However, we did not include it in this study because this sequence faces a significant challenge in brain applications because of its low encoding efficiency and hence a long scan time (>12 min) to achieve reliable stiffness maps.[11]

In the TURBINE-MRE experiments, we reduced the number of phase offsets to 4, trading that time for more EPI-blades in each image volume. This was helpful to exam the acceleration capability when retrospectively reducing the number of blades during reconstruction. In our standard MRE post-processing, we take the Fourier transfer in the time offset domain and only extract the first harmonic data for use in the stiffness calculations. Therefore, although the number of phase offsets was different between the SE-EPI-MRE and TURBINE-MRE experiments that does not change the first harmonic phase that is of interest.

In TURBINE-MRE acquisition, the phase-encoding direction of the TURBINE EPI blade is along the

superior-inferior direction (or z-direction) and different from that of SE-EPI-MRE (right-left direction or x-direction). Therefore, we will see more EPI-like artifact such as distortion and ghosting along z-direction in the coronal and sagittal planes, especially at the regions of high susceptibility variation such as the orbitofrontal and temporomesial brain areas.

The relatively long TE in the TURBINE-MRE sequence because of the presence of MEG could cause strong susceptibility artifacts and significant signal drop out. One may further reduce the TE using fractional motion encoding,[30] and/or multi-shot EPI for each blade. Alternatively, one may incorporate field effects into the acquired signal model and prospectively account for them during model-based iterative reconstruction (MBIR). This could be done either directly using an explicit field map model[31] or indirectly using a so-called point spread function (PSF) acquisition.[32,33]

Another limitation of the current sequence is that the TR time is restricted to the integer multiple of motion period (60 Hz or 80 Hz in this study) for synchronization, a delay time is needed after the sequence waveform, prolonging the scan time. To reduce the delay time, an interleaved phase offsets acquisition such as Ristretto[34] can be incorporated into the current sequence to further reduce scan time.

4 | CONCLUSION

This phantom and in vivo brain study demonstrated the feasibility of TURBINE-MRE for acquiring true 3D wave field data and stiffness map. With further development, this new MRE sequence has the potential to be highly accelerated for imaging fast dynamic stiffness changes and/or moving objects. Our pilot study encourages further exploration of TURBINE-MRE in, for example, functional MRE, free-breathing liver MRE, and cardiac MRE applications.

ORCID
Yi Sui (iD) https://orcid.org/0000-0002-8177-1661
Armando Manduca (iD) https://orcid.org/0000-0002-9411-5671

REFERENCES
1. Glaser KJ, Manduca A, Ehman RL. Review of MR elastography applications and recent developments. *J Magn Reson Imaging*. 2012;36:757-774.
2. Murphy MC, Huston J, Ehman RL. MR elastography of the brain and its application in neurological diseases. *NeuroImage*. 2019.187:176-183.
3. Schrank F, Warmuth C, Tzschatzsch H, et al. Cardiac-gated steady-state multifrequency magnetic resonance elastography of the brain: Effect of cerebral arterial pulsation on brain viscoelasticity. *J Cereb Blood Flow Metab*. 2020.40:991-1001.
4. Patz S, Fovargue D, Schregel K, et al. Imaging localized neuronal activity at fast time scales through biomechanics. *Sci Adv*. 2019;5:eaav3816
5. Lan PS, Glaser KJ, Ehman RL, Glover GH. Imaging brain function with simultaneous BOLD and viscoelasticity contrast: fMRI/fMRE. *Neuroimage*. 2020;211:116592.
6. McNab JA, Gallichan D, Miller KL. 3D steady-state diffusion-weighted imaging with trajectory using radially batched internal navigator echoes (TURBINE). *Magn Reson Med*. 2010;63:235-242.
7. Graedel NN, McNab JA, Chiew M, Miller KL. Motion correction for functional MRI with three-dimensional hybrid radial-Cartesian EPI. *Magn Reson Med*. 2017.78:527-540.
8. Jonathan SV, Vakil P, Jeong YI, Menon RG, Ansari SA, Carroll TJ. RAZER: A pulse sequence for whole-brain bolus tracking at high frame rates. *Magn Reson Med*. 2014;71:2127-2138.
9. Magnusson M, Leinhard OD, Brynolfsson P, Thyr P, Lundberg P. 3D magnetic resonance imaging of the human brain — Novel radial sampling, filtering and reconstruction. In: 12th IASTED International Conference on Signal and Image Processing (SIP 2010): ACTA Press; 2010. p Track-710.
10. Feng L, Axel L, Chandarana H, Block KT, Sodickson DK, Otazo R. XD-GRASP: Golden-angle radial MRI with reconstruction of extra motion-state dimensions using compressed sensing. *Magn Reson Med*. 2016;75:775-788.
11. Arani A, Grimm R, Trzasko J, et al. High resolution 3D GRE brain MR elastography is feasible with a high performance compact 3T scanner. *ISMRM*. 2017;25:1367.
12. Weavers PT, Shu YH, Tao SZ, et al. Technical note: Compact three-tesla magnetic resonance imager with high-performance gradients passes ACR image quality and acoustic noise tests. *Med Phys*. 2016;43:1259-1264.
13. Tan ET, Lee SK, Weavers PT, et al. High slew-rate head-only gradient for improving distortion in echo planar imaging: Preliminary experience. *J Magn Reson Imaging*. 2016;44:653-664.
14. Foo TKF, Laskaris E, Vermilyea M, et al. Lightweight, compact, and high-performance 3T MR system for imaging the brain and extremities. *Magn Reson Med*. 2018;80:2232-2245.
15. Bruder H, Fischer H, Reinfelder HE, Schmitt F. Image reconstruction for echo planar imaging with nonequidistant k-space sampling. *Magn Reson Med*. 1992;23:311-323.
16. Hinks RS, Mock BJ, Collick BD, Frigo FJ, Shubhachint T. Method and system for image artifact reduction using nearest-neighbor phase correction for echo planar imaging. U.S. Patent No. 7,102,352. 2006.
17. King KF, Angelos L. SENSE image quality improvement using matrix regularization. Proceedings of the 9th Annual Meeting of ISMRM, Glasgow, Scotland, 2001. p 1771.
18. Pruessmann KP, Weiger M, Bornert P, Boesiger P. Advances in sensitivity encoding with arbitrary k-space trajectories. *Magn Reson Med*. 2001;46:638-651.
19. Fessler JA, Sutton BP. Nonuniform fast Fourier transforms using min-max interpolation. *IEEE T Signal Process*. 2003;51:560-574.
20. Manduca A, Oliphant TE, Dresner MA, et al. Magnetic resonance elastography: Non-invasive mapping of tissue elasticity. *Med Image Anal*. 2001;5:237-254.

21. Murphy MC, Huston J 3rd, Jack CR Jr., et al. Measuring the characteristic topography of brain stiffness with magnetic resonance elastography. *PLoS One*. 2013;8:e81668.

22. Murphy MC, Huston J 3rd, Glaser K, Manduca A, Felmlee J. Phase correction for interslice discontinuities in multislice EPI MR elastography. *Montreal*. 2012;3426.

23. Stein CM. Estimation of the mean of a multivariate normal distribution. *Ann Stat*. 1981;9:1135-1151.

24. Arani A, Glaser KL, Arunachalam SP, et al. In vivo, high-frequency three-dimensional cardiac MR elastography: Feasibility in normal volunteers. *Magn Reson Med*. 2017.77:351-360.

25. Murphy IG, Graves MJ, Reid S, et al.. Comparison of breath-hold, respiratory navigated and free-breathing MR elastography of the liver. *Magn Reson Imaging*. 2017;37:46-50.

26. Uecker M, Lai P, Murphy MJ, et al. ESPIRiT–an eigenvalue approach to autocalibrating parallel MRI: Where SENSE meets GRAPPA. *Magn Reson Med*. 2014;71:990-1001.

27. Barnhill E, Hollis L, Sack I, et al. Nonlinear multiscale regularisation in MR elastography: Towards fine feature mapping. *Med Image Anal*. 2017;35:133-145.

28. Barnhill E, Nikolova M, Ariyurek C, Dittmann F, Braun J, Sack I. Fast Robust Dejitter and interslice discontinuity removal in MRI phase acquisitions: Application to magnetic resonance elastography. *IEEE Trans Med Imaging*. 2019;38:1578-1587.

29. Yin Z, Romano AJ, Manduca A, Ehman RL, Huston J 3rd. Stiffness and beyond: What MR elastography can tell us about brain structure and function under physiologic and pathologic conditions. *Top Magn Reson Imaging*. 2018;27:305-318.

30. Rump J, Klatt D, Braun J, Warmuth C, Sack I. Fractional encoding of harmonic motions in MR elastography. *Magn Reson Med*. 2007;57:388-395.

31. Sutton BP, Noll DC, Fessler JA. Fast, iterative image reconstruction for MRI in the presence of field inhomogeneities. *IEEE Trans Med Imaging*. 2003;22:178-188.

32. Robson MD, Gore JC, Constable RT. Measurement of the point spread function in MRI using constant time imaging. *Magn Reson Med*. 1997;38:733-740.

33. Zaitsev M, Hennig J, Speck O. Point spread function mapping with parallel imaging techniques and high acceleration factors: Fast, robust, and flexible method for echo-planar imaging distortion correction. *Magn Reson Med*. 2004;52:1156-1166.

34. Guenthner C, Sethi S, Troelstra M, Dokumaci AS, Sinkus R, Kozerke S. Ristretto MRE: A generalized multi-shot GRE-MRE sequence. *NMR Biomed*. 2019;32:e4049.

SUPPORTING INFORMATION

Additional Supporting Information may be found online in the Supporting Information section.

FIGURE S1 Scatter plots of median regional stiffness values when using the different number of blades for reconstruction. Stiffness obtained with ≥64 blades is almost identical to the one with 192 blades (r 0.999)